Molecular Catalysis 447 (2018) 21–27

Contents lists available at ScienceDirect

Molecular Catalysis

journal homepage: www.elsevier.com/locate/mcat

Gold catalysts supported on TiO_2-nanotubes for the selective hydrogenation of *p*-substituted nitrobenzenes

Cecilia C. Torres[a,*], Verónica A. Jiménez[a], Cristian H. Campos[b], Joel B. Alderete[c], Robinson Dinamarca[b], Tatiana M. Bustamente[b], Barbara Pawelec[d]

[a] Departamento de Ciencias Químicas, Facultad de Ciencias Exactas, Universidad Andres Bello, Sede Concepción, Autopista Concepción-Talcahuano 7100, Talcahuano, Chile
[b] Departamento de Fisicoquímica, Facultad de Ciencias Químicas, Universidad de Concepción, Edmundo Larenas 129, Casilla 160-C, Concepción, Chile
[c] Departamento de Química Orgánica, Facultad de Ciencias Químicas, Universidad de Concepción, Edmundo Larenas 129, Casilla 160-C, Concepción, Chile
[d] Instituto de Catálisis y Petroleoquímica (ICP-CSIC), Grupo de Energía y Química Sostenible (EQS), c/Marie Curie s/n Cantoblanco, Madrid, Spain

ARTICLE INFO

Article history:
Received 13 October 2017
Received in revised form 6 December 2017
Accepted 28 December 2017

Keywords:
Titania nanotubes
Gold nanoparticles
Nitrobenzenes
Selective hydrogenation
Multivariate regression

ABSTRACT

Gold nanoparticles supported on titania nanotubes (TiO_2NT) were synthesized and employed as an efficient catalysts for the selective hydrogenation of nitrobenzenes. Materials characterization by N_2 adsorption-desorption isotherms, XRD, HRTEM, DRS UV–vis, and XPS revealed that structured materials with high metal dispersion were obtained. The catalytic properties of these materials were tested using nitrobenzene and eight *p*-substituted analogs as model compounds with the aim of gaining insight into the role of electron-withdrawing and electron-donating substituents on the rate and selectivity of hydrogenation to the corresponding *p*-substituted anilines. Catalytic data showed pseudo first order kinetics for all compounds, with minimum formation of reaction intermediates and absence of condensation side products. Quantum chemical computational calculations demonstrated that the experimental kinetic constants (k) for the series of nitrobenzenes under study were described by a multilinear regression equation using the substituent Hammet sigma constant (σ), and the calculated solvation energy of the reactants (ΔG_{solv}) as predictor variables. The catalyst activity-structure correlation revealed that electronic effects are critical for the reaction kinetics, and that electron-withdrawing groups increase the hydrogenation rates over electron-donating substituents. Solvation plays also a relevant role as less solvated species interact better with the catalyst surface and react faster than highly solvated substrates. These results are valuable to design novel efficient strategies for the selective hydrogenation of nitrocompounds.

1. Introduction

Heterogeneous catalytic hydrogenation reactions are versatile chemical processes with a diversity of industrial applications in the production of pharmaceuticals, fine chemicals, fragrances, and agrochemicals, among others [1]. These reactions are highly selective, efficient, environmentally friendly, and cheaper compared to homogeneous procedures as the catalyst can often be recovered and recycled [2]. Currently, heterogeneous catalytic hydrogenation is the preferred choice for large scale reduction of nitrobenzenes, and 95% of the aromatic amines of industrial importance are obtained by this method, and continuous efforts are being developed in the search for novel catalyst for the efficient and selective hydrogenation of nitrocompounds [3–7].

A series of metals have been used as active phase for the reduction of nitrocompounds such as: Pd [8], Ni [9], Ir [10], Ag [11], Rh [12,13], and Au [14]. Within these species, Au nanoparticles have shown a remarkable catalytic potential due to the high affinity of this metal to the nitro group, thus providing an extraordinary ability to produce a rapid reduction to the corresponding amine with minimum traces of unwanted side products [15–20]. Further optimization of the catalytic performance of Au nanoparticles can be achieved by the physical entrapment of the active phase within nanoscale structured materials [21,22] such as metal oxide nanotubes, which have emerged as versatile platforms for catalytic and biomedical applications. Metal oxide nanotubes have gained great prominence for supporting metallic active phases due their high surface area, and fascinating electronic, magnetic, mechanical, and

* Corresponding author.
E-mail address: ceciliatorres.unab@outlook.com (C.C. Torres).

https://doi.org/10.1016/j.mcat.2017.12.039
2468-8231/

textural properties [23]. These features enable a narrow particle size distribution for the active phase and a high catalytic efficiency and selectivity, as recently reported by Duan et al. for the hydrogenation of nitrobenzene with Pd entrapped into SBA-15 [22,24]. Among metal oxide nanomaterials, titania nanotubes (TiO_2NTs) are exceptional candidates for catalytic applications due to its high chemical stability, large specific surface area, eco-friendly properties, and high surface functionality [25,26]. Additionally, TiO_2NTs provide a suitable framework for the efficient dispersion of the metal active phase [27,28]. Based on this background, the use of TiO_2NTs as support for Au nanoparticles appears as a valuable strategy to improve the catalytic performance of this metal in hydrogenation reactions of nitrobenzenes, as studied in the present report.

In this work, TiO_2NTs were prepared by hydrothermal synthesis using an alkali treatment of TiO_2 nanoparticles. This material was used to support Au nanoparticles synthetized by deposition-precipitation method. The Au-TiO_2NT system was tested as catalyst for the selective hydrogenation of a series *para*-substituted nitrobenzenes using semi-batch conditions in ethanol liquid phase [5]. Compounds under study contain electron-withdrawing and electron-donating groups in the *p*-position relative to the nitro moiety, aimed at examining the role of electronic effects on the catalytic performance of the Au-TiO_2NT system. Kinetic data (log k) was modeled using a multilinear regression equation, in which the Hammet's sigma constants (σ) of the *p*-substituents, and the DFT-calculated solvation energy of the reactants in ethanol were employed as predictor variables.

2. Experimental

2.1. Reagents

All reagents were purchase and used as received. The synthesis of TiO_2NTs was performed using titanium oxide anatase nanoparticles (nanopower, particle size <25 nm, BET surface area 45–55 $m^2\,g^{-1}$), sodium hydroxide (NaOH, Merck) and HNO_3 (Merck, 65%). Gold(III) chloride trihydrate (Sigma-Aldrich 99.9%), nitrobenzene (Ph-NO_2), *p*-nitrotoluene (*p*-CH_3), *p*-nitrophenol (*p*-OH, Merck), *p*-nitroaniline (*p*-NH_2, Merck), *p*-dinitrobenzene (*p*-NO_2, Sigma-Aldrich), *p*-nitrobenzonitrile (*p*-CN, Fluka), *p*-nitroanisol (*p*-OCH_3, Sigma-Aldrich), *p*-nitrobenzaldehyde (*p*-CHO) and *p*-chloronitrobenzene (*p*-Cl, Merck), absolute ethanol (Merck), and H_2 by AGA, Chile.

2.2. TiO_2NT synthesis

The synthesis of TiO_2NTs was performed using a hydrothermal process [29]. For this purpose, 2.5 g of the TiO_2 nanoparticles was dispersed in 125 mL of 10 mol·L^{-1} NaOH. The mixture was placed into a hydrothermal reactor at 110 °C for 24 h with constant agitation. After the hydrothermal treatment the solid was washed with distilled water and put in contact with a 0.10 mol·L^{-1} solution of HNO_3 overnight at room temperature. The mixture was washed and filtered with distilled water and the obtained nanotubes were dried at room temperature for the night and then at 100 °C for 12 h.

2.3. Deposition-precipitation of Au nanoparticles with NaOH at 100 °C

Gold nanoparticles synthesis was performed using a deposition-precipitation method [14]. The appropriate amount of TiO_2NT was placed in a round bottom flask together with 50 mL of water. Subsequently, the required amount of $HAuCl_4$ for 1.0% wt. Au was added together with a stoichiometric amount of NaOH (0.10 mol L^{-1}). After connecting a flux of H_2 to the round bottom flask containing the mixture, the system was heated to reflux at 80 °C under stirring until the change of color from yellow to purple. The adsorbed anionic complex $[AuCl_2(OH)_2]^-$ was decomposed under flowing hydrogen forming Au^0. The solid was filtered and dried for 2 h at 100 °C, and labeled as Au-TiO_2NT.

2.4. Materials characterization

The characterization of TiO_2NT and Au-TiO_2NT systems was conducted using the following techniques. N_2 adsorption-desorption isotherms were carried out in an ASAP 2010 Micromeritics apparatus. Pore-size distributions were calculated from the N_2 adsorption branch using the Barrett-Joyner-Halenda model (BJH). X-ray diffraction (XRD) was performed on a Rigaku X-ray Geigerflex diffractometer using a Ni filter and Cu K α radiation within 2–80° 2θ range. HRTEM was performed using a Philips CM200 model high resolution electron microscope with energy dispersive analyzer and digital camera coupled to a high speed TVIPS FastScan F-114 model of 1024 × 1024 pixels and 12 bits. Metal particles were counted, and the surface area-weighted mean Au diameter (d_p) was calculated using the following equation:

$$d_p = \frac{\sum_i n_i d_i^3}{\sum_i n_i d_i^2} \quad (1)$$

UV–vis spectra of diffuse reflectance of solid state was studied in the range of 200–900 nm on a Varian Cary 3 UV–vis spectrophotometer equipped with an area of 150 mm in diameter covered with poly integration tetra-fluoroethylene (PTFE). The dust samples were mounted in a quartz cell, which provided a sample thickness greater than 3 mm and thus guaranteed "infinite" sample thickness. Chemical analysis was performed by inductively coupled plasma-mass spectrometry on an ICP-MS Spectrometer Perkin Elmer Elas 6000. Photoelectron spectra (XPS) were recorded using an Escalab 200R spectrometer provided with a hemispherical analyzer, operated in a constant pass energy mode and Mg Kα X-ray radiation ($h\nu$ = 1253.6 eV) operated at 10 mA and 12 kV.

2.5. Liquid phase hydrogenation of nitrobenzenes

The catalytic assays of nitrobenzenes hydrogenation were performed in a stainless steel (150 mL) Parr-type semi-batch reactor at a 25 °C using 0.100 g of catalyst and 0.02 mol·L^{-1} of nitrobenzene as model molecule in ethanol, under 40 bar hydrogen pressure. All the components (catalyst, solvent and substrate) were fed to the reactor and stirred at 700 rpm. No mass transfer resistance were found in a catalytic test established using the Madon and Boudart approach [30]. No catalytic activity for pure TiO_2NT was confirmed in a blank test. Pseudo-first-order kinetic constants (k) were calculated as reported in previous studies [31]. Analytical quantifications for reactants and products were analyzed by gas chromatography using a GC–MS Shimadzu GCMS-QP5050 with a capillary column β-Dex 225 (Supelco).

2.6. Solvation energy calculations

Quantum chemical computational calculations were employed to estimate the solvation energy of the series of nitrobenzenes under study. Geometry optimization and solvation energy calculations were computed under the frame of Density Functional Theory (DFT) using the Gaussian 09 program. The hybrid B3LYP functional was employed, which includes Beckeís 3-parameter nonlocal-exchange functional [32] with the correlation functional of Lee et al. [33]. The basis set employed for the calculations was 6–311G(2p,2d). No symmetry constrains were applied during geometry optimization procedures. Solute solvation energies

(ΔG_S) were computed using the standard polarizable continuum model (PCM) in ethanol and expressed as the difference between the solute energy in ethanol solution and the solute energy in gas phase.

3. Results and discussion

Titanium oxide nanotubes (TiO_2NT) were employed as support for Au nanoparticles, aimed at developing a novel catalytic system for the selective reduction of a series of *p*-substituted nitrobenzenes to the corresponding anilines. TiO_2NT were synthesized following a hydrothermal procedure, whereas Au incorporation was achieved by deposition-precipitation under alkaline conditions, using NaOH as a precipitation agent. The prepared Au-TiO_2NT material was subjected to exhaustive characterization procedures as detailed next.

3.1. Morphology and textural properties of TiO_2NT and Au-TiO_2NT materials

The initial characterization of TiO_2NTs was performed by N_2 adsorption isotherms at −196 °C, which showed a typical type IV profile according to the IUPAC classification corresponding to a mesoporous material with cylindrical pores [34]. The hysteresis loop revealed the existence of large pores that are not being filled [35] and intermediate mesoporous of H1 and H3 types. The specific area calculated from the BET method was 313 $m^2\,g^{-1}$, with average pore diameter of 10.2 nm determined from the BJH method, and a total pore volume of 0.66 $cm^3\,g^{-1}$ measured at P/P_o = 0.99. The textural properties of TiO_2NTs were considered appropriate to proceed with the incorporation of Au nanoparticles thus producing the Au-TiO_2NT system for catalytic applications. The Au content in the Au-TiO_2NT was estimated from ICP-MS analysis revealing a metal content of 0.54% wt. This amount is approximately 60% of the nominal Au content, which can be explained due to leaching of metal nanoparticles during the synthetic procedure, as reported in the literature [36].

X-ray diffraction was employed to confirm the conversion of TiO_2-anatase to TiO_2NT as shown in Fig. 1A. Characteristic diffractions lines for TiO_2-anatase phase were observed at 2θ 25.4°, 37.9° and 48.2°, whereas TiO_2NTs exhibited broader peaks, with characteristics diffraction patters at 2θ 25°, 29.9° and 48°, which are associated to the trititanate phase of the solid [37–39]. In the case of the Au-TiO_2NT system, XRD patterns reveal that the support structure remains unaltered after the deposition of Au nanoparticles. The reflection lines of metallic Au are clear and associated to Miller indices of (1 1 1) and (2 0 0).

DRS UV–vis data for TiO_2-anatase, TiO_2NT, and Au-TiO_2NT systems is presented in Fig. 1B, showing an absorption band around 200–400 nm, which was attributed to the intrinsic band gap of TiO_2-based materials [40]. For TiO_2-anatase two peaks at 270 and 320 nm were observed, whereas TiO_2NTs showed only one peak at 250 nm indicating the different shape of this system compared anatase nanoparticles. In the case of the Au-TiO_2NT system, a visible-light absorption in the region ranging from 500 nm to 600 nm is observed due to localized surface plasmon resonance of Au nanoparticles. The plasmon centered at 580 nm [41–43] indicates that Au nanoparticles are mostly spherical. The intensity and width of the plasmon depends on the particle size indicating a size distribution for the catalyst [44–47].

Morphology of the Au-TiO_2NT system was confirmed by HR-TEM, showing a well-defined tubular structure with average length of 57 nm and external diameter of 8.5 nm. Au nanoparticles of spherical shape were detected from the HR-TEM micrograph, distributed inside the tubular structure and on the outer surface of the NTs, in agreement with DRS UV–vis data. An average Au particle size of 5.5 ± 1.3 (nm) was measured from HR-TEM, with a dispersion of 18%. Smaller Au spheres were preferably found in the interior of the nanotubular structures. No remains of TiO_2 nanoparticles were detected in the micrograph, thus proving the high yield conversion to TiO_2NTs under the experimental conditions.

The XPS spectrum of the Au-TiO_2NT system is shown in Fig. 1D. The curve fitting of the Au core-level spectrum was performed by using a two spin-orbit split Au $4f_{7/2}$ and Au $4f_{5/2}$. Only the values of level $4f_{7/2}$ of gold were analyzed. For the Au-TiO_2NT system only one Au signal is present which is associated to pure metallic Au^0 species (Au$4f_{7/2}$ 83.9 eV) [48,49], thus confirming that the colloidal procedure allowed the metal to be obtained in the zero-valence state. Two energy values for oxygen were observed at 530.1 eV, corresponding to the Ti-O bond of the crystalline network, and at 531.6 eV, associated to Ti-OH groups on the surface of the support [50,51] or defective oxygens of the structure [52,53]. Ti 2p core level indicates the presence of Ti^{4+} state in the nanotubes with a binding energy of 458.6 (eV) [54]. The $(Au/Ti)_{at}$ ratio of the catalyst is approximately 0.0050, which shows a two-fold increase compared to the $(Au/Ti)_{bulk}$ ratio of 0.0022, thus indicating that the catalyst has higher dispersion in agreement with HR-TEM results.

3.2. Catalytic activity

The hydrogenation of nitrobenzene was used as model reaction to evaluate the catalytic activity of Au nanoparticles supported in TiO_2NTs. This reaction was carried out in ethanol at room temperature during 7 h, under conditions of 0.02 mol·L^{-1} substrate concentration, 40 bar of H_2 pressure, and 700 rpm stirring rate. The corresponding reaction profile is shown in Fig. 2. Our results revealed that the supported Au catalyst exhibited a high efficiency in the nitrobenzene hydrogenation reaction, showing a pseudo-first order kinetics respect to the substrate. During the reaction course, the formation of aniline (>90%) was highly favored over the accumulation of reaction intermediates (Fig. 2), showing that the Au-TiO_2NT system is a very selective catalyst for nitrobenzene hydrogenation, in agreement with the experimental findings reported by Combita et al. on a titania supported gold catalyst [55]. A relevant outcome regarding these results is that a high catalytic activity and a high selectivity towards hydrogenation to anilines was achieved by the Au-TiO_2NT system despite its low metal content. Two reaction intermediates were detected, namely nitrosobenzene and N-phenylhydroxylamine, with no evidence of condensation by products. [14,56]. Both intermediates were detected at very low concentrations, thus supporting the predominance of a direct hydrogenation route over a condensation route [55]. The formation of nitrosobenzene as a reaction intermediate supports a Haber reaction mechanism for the hydrogenation of nitrobenzene, in which a multi-step reaction path leads to the reduction of the nitro group to nitroso, and the subsequent formation of hydroxylamino and amino moieties. This mechanism has been reported to be favored under basic conditions, such as those found within TiO_2NTs, which tend to be more basic than their precursor. A new reaction mechanism was proposed by Jackson et al. [51], in which nitrosobenzene cannot be a reaction intermediate. This mechanism is expected to be favored under acidic conditions and high hydrogen supply. Nevertheless, there is still ongoing research regarding this issue, and the exact mechanism for the hydrogenation of nitrobenzene still remains as a matter of controversy. Regarding the rate-limiting step of the Haber reaction mechanism, Corma et al. [52] have reported that the reduction of phenylhydroxylamine to aniline is the rate-determining step of the whole process. To further obtain insight into the structural effects that govern the catalytic hydrogenation of nitrobenzene, a series of *p*-substituted nitrobenzenes were employed as substrates for

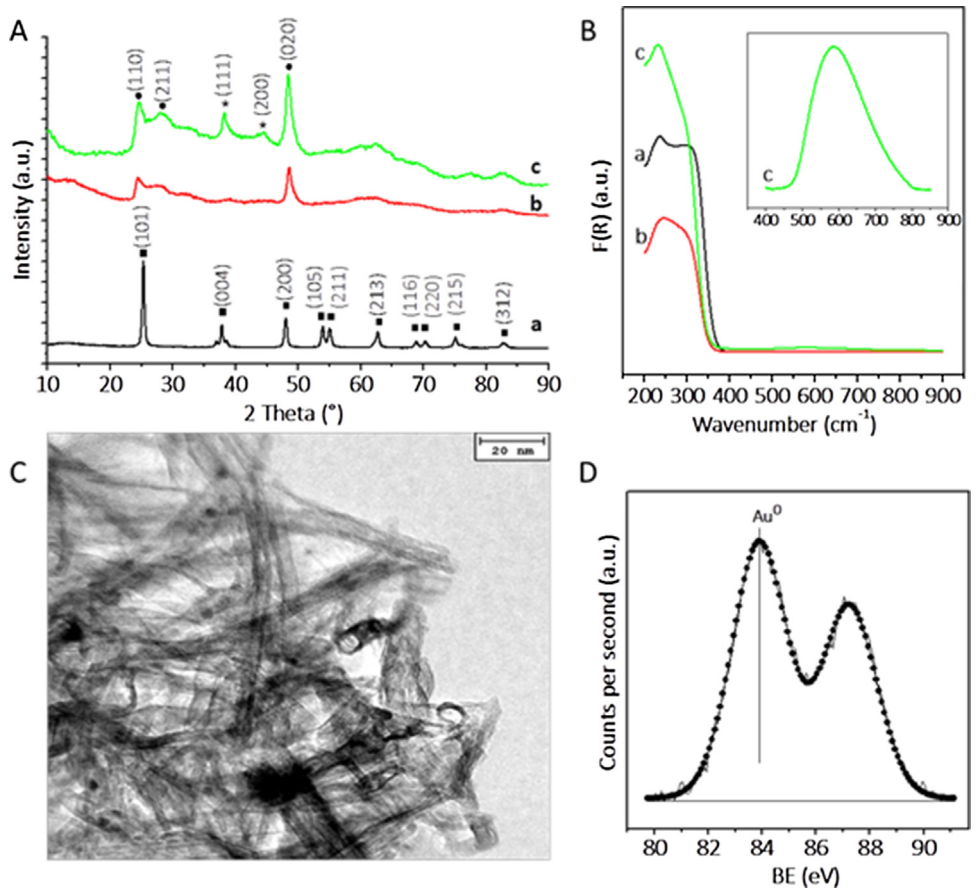

Fig. 1. (A) Diffraction patterns for a) TiO_2-anatase, b) TiO_2-NT and c) Au-TiO_2NT systems. Reference patterns (■) anatase (JCPDS: 00-021-1272) (•)$H_2Ti_4O_9$ x H_2O and (*) Au (JCPDS: 00-021-1272). (B) DRS UV–vis data for a) TiO_2-anatase, b) TiO_2-NT and c) Au-TiO_2NT systems. (C) HR-TEM micrograph for Au-TiO_2NT, and (D) XPS spectra of Au for Au-TiO_2NT catalyst.

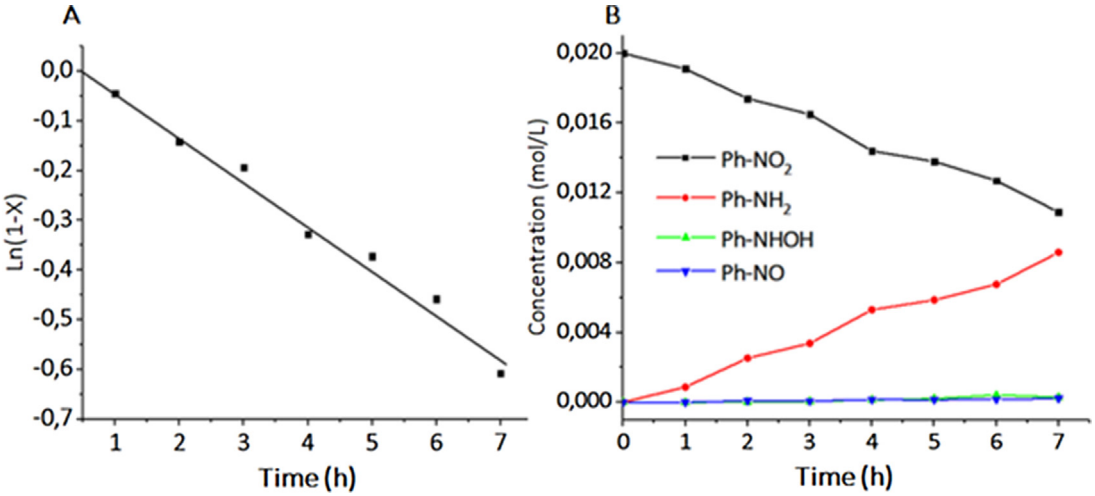

Fig. 2. (A) Reaction profile for the catalytic hydrogenation nitrobenzene, (B) Product and intermediates distribution for the hydrogenation of nitrobenzene.

this reaction, aimed at evaluating the role of electron-donating and electron-withdrawing groups in the rate of hydrogenation.

3.2.1. *Hydrogenation of* para-*substituted nitrobenzenes*

The catalytic hydrogenation of a series of *p*-substituted nitrobenzenes was carried out with the aim of gaining insight into the role of electronic effects on the reaction rate and selectivity towards the formation of the corresponding *p*-substituted anilines. To this purpose, four electron-withdrawing groups (—NO_2, —CHO, —CN, —Cl), and four electron-donating groups (—CH_3, —OCH_3, —OH, —NH_2) were considered in the present study. Kinetic data revealed that all compounds exhibited pseudo-first order constants for the catalytic hydrogenation reaction, leading to the formation of the corresponding *p*-substituted anilines as major products with yields higher than 89%, and minor proportions of detected reaction intermediates in all cases (Fig. 3). These results suggest that the Au catalyst supported in TiO_2NTs favor a direct route for the hydrogenation of nitrobenzene and *p*-substituted analogs, thus

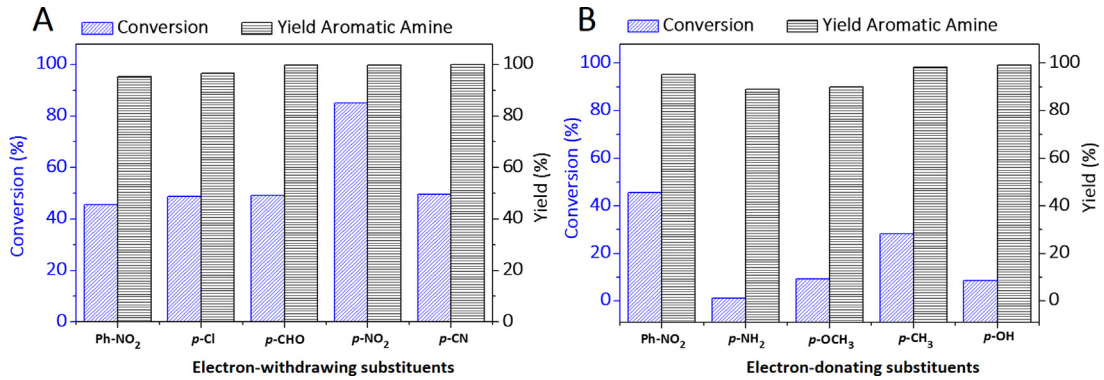

Fig. 3. Percentages of conversion and yield for the catalytic hydrogenation of *p*-substituted nitrobenzenes to the corresponding *p*-substituted anilines.

Table 1
Experimental pseudo-first order kinetic constants (k) for the catalytic hydrogenation of nitrobenzene and *p*-substituted nitrobenzenes over 1%Au/TiO_2NT catalyst. Estimated kinetic constants (k_{model}) were obtained from a multilinear regression model using the Hammet sigma constant (σ) and the solvation free energy of the substrate (ΔG_{sov}) as predictor variables. ΔG_{solv} were calculated at B3LYP/6-311G (2p,2d) level of theory.

Substituent	k ($h^{-1}g_{cat}^{-1}$)	k_{model}	σ	ΔG_{solv} (kcal/mol)
—H	0.792	0.714	0.00	−4.04
—Cl	1.273	1.677	0.11	−3.96
—CHO	1.444	1.137	0.73	−5.61
—NO_2	2.779	2.975	0.79	−5.74
—CN	1.275	1.533	0.66	−6.35
—NH_2	0.008	0.016	−1.30	−7.74
—OCH_3	0.181	0.258	−0.78	−4.48
—CH_3	0.460	0.390	−0.31	−4.25
—OH	0.123	0.061	−0.92	−6.75

suppressing the condensation route. Nevertheless, significant variations were observed in the conversion of the reactant to the desired product, and in the rate of hydrogenation as the electronic nature of the substituent group was modified, which evidenced a strong influence of electronic effects on this reaction (Table 1). Kinetic data revealed that electron-withdrawing groups activated the hydrogenation reaction, whereas electron-donating groups drastically reduced the rate of reaction compared to nitrobenzene. Within electron-withdrawing substituents, the —NO_2 group exerted the largest increase in the rate constant compared to —CHO, —CN, and —Cl moieties, which exhibited similar activating profiles. Additionally, the —NO_2 group induced a large increase in conversion to *p*-nitroaniline (80%) compared to nitrobenzene, which exhibited a 45% conversion to aniline, as detailed in Fig. 3. In the case of electron-donating groups, all species displayed reduced rate constants compared to nitrobenzene, following the sequence —CH_3 >—OCH_3 >—OH » —NH_2. The largest deactivating effect was displayed by the —NH_2 substituent, with the lowest kinetic constant and a minimum conversion of 1% to *p*-phenylenediamine. Strong electron-donating groups such as —OH and —OCH_3 induced also a decreased conversion to the corresponding *p*-substituted anilines, with conversion percentages close to 10%. The weak electron-donating —CH_3 group exhibited a less pronounced effect in conversion showing a 27% percentage of substrate transformation to *p*-toluidine.

The strong dependence between the hydrogenation rate and the nature of the substituents in the series of *p*-substituted nitrobenzenes under study can be explained in light of the proposed Haber reaction mechanism, in which the rate-limiting step involves the hydrogenation of N-phenyl hydroxylamine to the corresponding aniline, with the loss of a water molecule. A growing electron density on the N atom is expected to occur in the transition state of this rate-determining step [57], which can be stabilized by the presence

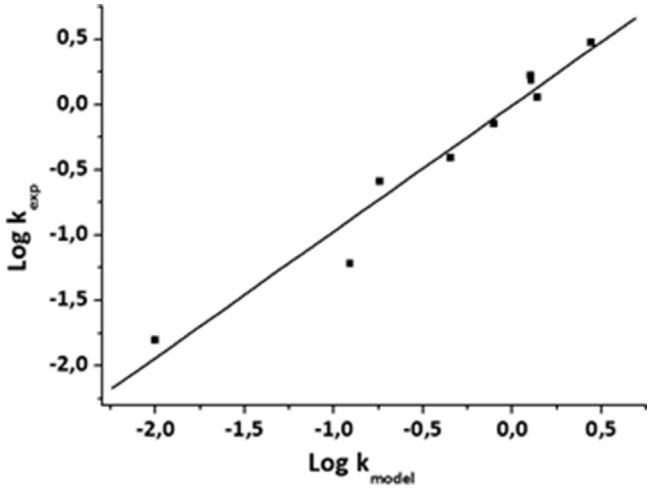

Fig. 4. Correlation between log k_{exp} and logk_{model} for *para*-substituted nitroarenes hydrogenation on Au/TiO_2NT catalyst. Conditions: a batch reactor, T = 25 °C, 40 bar of H_2 pressure, 0.02 mol L^{-1} nitrocompound concentration.

of electron-withdrawing groups in the aromatic ring. On the other hand, the presence of electron-donating groups exerts a destabilizing effect on the transition state of the rate-limiting reaction, thus explaining the sensitivity of this reaction to substituent effects.

To further provide a quantitative description for the structural dependence of hydrogenation rates, a multilinear regression model was built using the Hammet sigma constant (σ) of the substituent, and the solvation free energy (ΔG_{solv}) of the substrate as predictor variables. Under this approach, the σ parameters were employed as well-known descriptors of the electronic properties of the substituents in the *p*-position, whereas ΔG_{solv} values were used to describe the affinity of the substrate towards the solvent (ethanol), which might be critical for reactivity, since highly solvated species are more impeded to interact with the surface of the catalyst and thus will react slower than less solvated reactants. ΔG_{solv} values in ethanol were estimated from DFT computational calculations at B3LYP/6-311G (2p, 2d) level of theory using the standard PCM continuum solvation method. Our results revealed that the experimental pseudo-first order kinetic constants (k) for the hydrogenation of the series of *p*-substituted nitrobenzenes are described by the multilinear regression displayed in Eq. (1):

$$\log k = 0.747 + 1.276\sigma + 0.221\Delta G_S \quad (1)$$

A high correlation between experimental ($\log k$) and estimated ($\log k_{model}$) kinetic constants was attained with a squared regression coefficient of $r^2 = 0.970$ (Fig. 4). Variance analysis revealed that the most determinant variable is the σ parameter, thus indicat-

ing that electronic effects play a predominant role in determining the rate of hydrogenation of *p*-substituted nitrobenzenes. The regression coefficient corresponding to σ can be interpreted as ρ > 1 Hammet reaction constant, which is consistent with a highly structure-sensitive reaction in which negative charge is built during the rate-limiting step thus being favored by electron-withdrawing groups. On the other hand, the regression coefficient corresponding to ΔG_{solv} indicates that a high affinity towards the solvent reduces the reactivity of *p*-substituted nitrobenzenes upon hydrogenation, as expected. This also suggests that the catalytic hydrogenation of nitrobenzenes could be faster in a less polar environment. This is a relevant result considering that nitrobenzenes hydrogenation reactions are customarily performed in polar solvents such as methanol and ethanol [20,55,58,59]. Thus, our theoretical predictions provide the basis for future studies dealing with solvation effects on the catalytic performance of Au-TiO_2NT systems

4. Conclusions

Nanosize TiO_2NT were successfully prepared by hydrothermal synthesis, and employed as support for Au nanoparticles. Au deposition reached almost a 60% of metal content due to leaching during the catalyst synthesis. The Au/TiO_2NT catalyst was active and selective to the hydrogenation of *p*-substituted nitrobenzenes studied in liquid phase at room temperature. Pseudo-first-order kinetics with respect to the reactant were found in all cases. Selectivity of the catalyst towards *p*-substituted anilines reached 90% for all substrates under study, thus favoring the formation of aromatic amines over the accumulation of reaction intermediates. The absence of condensation side products revealed that the mechanism of nitrobenzenes hydrogenation followed a direct route in which the formation of negative charge in the transition state of the rate-limiting step is expected. The catalytic efficiency was promoted by electron-withdrawing substituents, as revealed by the strong correlation between the Hammett σ constant of the substitutent and the experimental kinetic constants for the series of *p*-substituted nitrobenzenes under study. A multilinear regression analysis was carried out to account for the variation of hydrogenation rates within the set of compounds under study in terms of the Hammett σ constant and calculated solvation energies for the reactants. Our results revealed that electronic effects are critical to modulate the rate of hydrogenation and that highly solvated species are less reactive upon catalytic hydrogenation. These results are valuable to design novel more efficient synthetic strategies for the selective hydrogenation of nitrocompounds.

Acknowledgements

The authors thank the Project FONDECYT 11160468 and R. Dinamarca thanks CONICYT for his doctoral fellowship N° 21150092 and T. Bustamente thanks Universidad de Concepción for his doctoral fellowship.

Appendix A. Supplementary data

Supplementary data associated with this article can be found, in the online version, at http://dx.doi.org/10.1016/j.mcat.2017.12.039.

References

[1] X. Yang, L. Wu, L. Ma, X. Li, T. Wang, S. Liao, Pd nano-particles (NPs) confined in titanate nanotubes (TNTs) for hydrogenation of cinnamaldehyde, Catal. Commun. 59 (2015) 184–188.
[2] H.U. Blaser, F. Spindler, M. Studer, Appl. Catal. A 221 (2001) 119–143.
[3] Q. Xiao, S. Sarina, E.R. Waclawik, J. Jia, J. Chang, J.D. Riches, H. Wu, Z. Zheng, H. Zhu, Alloying gold with copper makes for a highly selective visible-light photocatalyst for the reduction of nitroaromatics to anilines, ACS Catal. 6 (2016) 1744–1753.
[4] S. Zhang, C.-R. Chang, Z.-Q. Huang, J. Li, Z. Wu, Y. Ma, Z. Zhang, Y. Wang, Y. Qu, High catalytic activity and chemoselectivity of sub-nanometric Pd clusters on porous nanorods of CeO2 for hydrogenation of nitroarenes, J. Am. Chem. Soc. 138 (2016) 2629–2637.
[5] T.Y. Yang, L.J. Wei, L.Y. Jing, J.F. Liang, X.M. Zhang, M. Tang, M.J. Monteiro, Y. Chen, Y. Wang, S. Gu, D.Y. Zhao, H.Q. Yang, J. Liu, G.Q.M. Lu, Dumbbell-shaped Bi-component mesoporous janus solid nanoparticles for biphasic interface catalysis, Angew. Chem. Int. Ed. 56 (2017) 8459–8463.
[6] W.J. Zhang, L.M. Fu, H.Q. Yang, Micrometer-scale mixing with pickering emulsions: biphasic reactions without stirring, Chemsuschem 7 (2014) 391–396.
[7] H.F. Liu, Z.M. Zhang, H.Q. Yang, F.Q. Cheng, Z.P. Du, Recycling nanoparticle catalysts without separation based on a pickering emulsion/organic biphasic system, Chemsuschem 7 (2014) 1888–1900.
[8] M. Tian, X. Cui, C. Dong, Z. Dong, Palladium nanoparticles dispersed on the hollow aluminosilicate microsphere@hierarchical γ-AlOOH as an excellent catalyst for the hydrogenation of nitroarenes under ambient conditions, Appl. Surf. Sci. 390 (2016) 100–106.
[9] Y. Shu, S. He, L. Xie, H.C. Chan, X. Yu, L. Yang, Q. Gao, Ni/Mo2C nanowires and their carbon-coated composites as efficient catalysts for nitroarenes hydrogenation, Appl. Surf. Sci. 396 (2017) 339–346.
[10] C. Campos, C. Torres, M. Oportus, M.A. Peña, J.L.G. Fierro, P. Reyes, Hydrogenation of substituted aromatic nitrobenzenes over 1 wt.%Ir/ZrO2 catalyst: effect of meta position and catalytic performance, Catal. Today 213 (2013) 93–100.
[11] F. Cárdenas-Lizana, Z.M. de Pedro, S. Gómez-Quero, M.A. Keane, Gas phase hydrogenation of nitroarenes: a comparison of the catalytic action of titania supported gold and silver, J. Mol. Catal. A: Chem. 326 (2010) 48–54.
[12] S.M. Baghbanian, M. Farhang, S.M. Vahdat, M. Tajbakhsh, Hydrogenation of arenes, nitroarenes, and alkenes catalyzed by rhodium nanoparticles supported on natural nanozeolite clinoptilolite, J. Mol. Catal. A: Chem. 407 (2015) 128–136.
[13] C.H. Campos, E. Rosenberg, J.L.G. Fierro, B.F. Urbano, B.L. Rivas, C.C. Torres, P. Reyes, Hydrogenation of nitro-compounds over rhodium catalysts supported on poly[acrylic acid]/Al2O3 composites, Appl. Catal. A 489 (2015) 280–291.
[14] C.C. Torres, J.B. Alderete, G. Pecchi, C.H. Campos, P. Reyes, B. Pawelec, E.G. Vaschetto, G.A. Eimer, Heterogeneous hydrogenation of nitroaromatic compounds on gold catalysts: influence of titanium substitution in MCM-41 mesoporous supports, Appl. Catal. A 517 (2016) 110–119.
[15] J. Zhou, J. Ralston, R. Sedev, D.A. Beattie, Functionalized gold nanoparticles: synthesis, structure and colloid stability, J. Colloid Interface Sci. 331 (2009) 251–262.
[16] M. Haruta, T. Kobayashi, H. Sano, N. Yamada, Chem. Lett. (1987) 405–408.
[17] Y. Li, S. Liu, T. Yao, Z. Sun, Z. Jiang, Y. Huang, H. Cheng, Y. Huang, Y. Jiang, Z. Xie, G. Pan, W. Yan, S. Wei, Controllable synthesis of gold nanoparticles with ultrasmall size and high monodispersity via continuous supplement of precursor, Dalton Trans. 41 (2012) 11725–11730.
[18] C. Torres, C. Campos, J.L.G. Fierro, M. Oportus, P. Reyes, Nitrobenzene hydrogenation on Au/TiO2 and Au/SiO2 catalyst: synthesis, characterization and catalytic activity, Catal. Lett. 143 (2013) 763–771.
[19] C.C. Torres, J.B. Alderete, G. Pecchi, C.H. Campos, P. Reyes, B. Pawelec, E.G. Vaschetto, G.A. Eimer, Heterogeneous hydrogenation of nitroaromatic compounds on gold catalysts: influence of titanium substitution in MCM-41 mesoporous supports, Appl. Catal. A: Gen. 517 (2016) 110–119.
[20] P. Serna, A. Corma, Transforming nano metal nonselective particulates into chemoselective catalysts for hydrogenation of substituted nitrobenzenes, ACS Catal. 5 (2015) 7114–7121.
[21] W. Chen, Z. Fan, X. Pan, X. Bao, Effect of confinement in carbon nanotubes on the activity of fischer-tropsch iron catalyst, J. Am. Chem. Soc. 130 (2008) 9414–9419.
[22] Y. Duan, M. Zheng, D. Li, D. Deng, C. Wu, Y. Yang, Synthesis of Pd/SBA-15 catalyst employing surface-bonded vinyl as a reductant and its application in the hydrogenation of nitroarenes, RSC Adv. 7 (2017) 3443–3449.
[23] H.-H. Ou, S.-L. Lo, Review of titania nanotubes synthesized via the hydrothermal treatment: fabrication, modification, and application, Sep. Purif. Technol. 58 (2007) 179–191.
[24] L. Jiang, H. Gu, X. Xu, X. Yan, Selective hydrogenation of o-chloronitrobenzene (o-CNB) over supported Pt and Pd catalysts obtained by laser vaporization deposition of bulk metals, J. Mol. Catal. A: Chem. 310 (2009) 144–149.
[25] T. Wang, J. Wei, H. Shi, M. Zhou, Y. Zhang, Q. Chen, Z. Zhang, Preparation of electrospun Ag/TiO2 nanotubes with enhanced photocatalytic activity based on water/oil phase separation, Physica E 86 (2017) 103–110.
[26] G. Zhang, H. Miao, X. Hu, J. Mu, X. Liu, T. Han, J. Fan, E. Liu, Y. Yin, J. Wan, A facile strategy to fabricate Au/TiO2 nanotubes photoelectrode with excellent photoelectrocatalytic properties, Appl. Surf. Sci. 391 (Part B) (2017) 345–352.
[27] X. Yang, X. Yu, L. Long, T. Wang, L. Ma, L. Wu, Y. Bai, X. Li, S. Liao, Pt nanoparticles entrapped in titanate nanotubes (TNT) for phenol hydrogenation: the confinement effect of TNT, Chem. Commun. 50 (2014) 2794–2796.
[28] X. Yang, W. Wang, L. Wu, X. Li, T. Wang, S. Liao, Effect of confinement of TiO2 nanotubes over the Ru nanoparticles on Fischer-Tropsch synthesis, Appl. Catal. A 526 (2016) 45–52.

[29] C.C. Torres, C.H. Campos, C. Diáz, V.A. Jiménez, F. Vidal, L. Guzmán, J.B. Alderete, PAMAM-grafted TiO2 nanotubes as novel versatile materials for drug delivery applications, Mater. Sci. Eng. C 65 (2016) 164–171.
[30] M. Boudart, Adv. Catal. 20 (1969) 153–166.
[31] C.H. Campos, M. Jofré, C.C. Torres, B. Pawelec, J.L.G. Fierro, P. Reyes, Chemoselective hydrogenation of o-, p- and m-chloronitrobenzene at ambient temperature on Au/Fe2O3 catalysts, Appl. Catal. A 482 (2014) 127–136.
[32] A.D. Becke, Density-functional thermochemistry. III. The role of exact exchange, J. Chem. Phys. 98 (1993) 5648–5652.
[33] C. Lee, W. Yang, R.G. Parr, Development of the Colle-Salvetti correlation-energy formula into a functional of the electron density, Phys. Rev. B 37 (1988) 785–789.
[34] D. Wang, B. Yu, F. Zhou, C. Wang, W. Liu, Mater. Chem. Phys. 113 (2009) 602–606.
[35] D.V. Bavykin, V.N. Parmon, A.A. Lapkin, F.C. Walsh, The effect of hydrothermal conditions on the mesoporous structure of TiO2 nanotubes, J. Mater. Chem. 14 (2004) 3370–3377.
[36] C.L. Rodolfo Zanella, Suzanne Giorgio, Raymonde Touroude, J. Catal. 223 (2004) 328–339.
[37] Q. Chen, G.H. Du, S. Zhang, L.M. Peng, The structure of trititanate nanotubes, Acta. Crystallogr. B 58 (2002) 587–593.
[38] J. Yang, Z. Jin, X. Wang, W. Li, J. Zhang, S. Zhang, X. Guo, Z. Zhang, Study on composition, structure and formation process of nanotube Na2Ti2O4(OH)2, Dalton Trans. (2003) 3898–3901.
[39] G. Armstrong, A.R. Armstrong, J. Canales, P.G. Bruce, Nanotubes with the TiO2-B structure, Chem. Commun. (2005) 2454–2456.
[40] L. Wu, F. Li, Y. Xu, J.W. Zhang, D. Zhang, G. Li, H. Li, Plasmon-induced photoelectrocatalytic activity of Au nanoparticles enhanced TiO2 nanotube arrays electrodes for environmental remediation, Appl. Catal. B 164 (2015) 217–224.
[41] C.F. Bohren, D.R. Huffman, Absorption and Scattering of Light by Small Particles, John Wiley, New York, 1983.
[42] M. Kerker, The Scattering of Light and Other Electromagnetic Radiation, Academic Press, New York, 1969.
[43] R. Fenger, E. Fertitta, H. Kirmse, A.F. Thunemann, K. Rademann, Size dependent catalysis with CTAB-stabilized gold nanoparticles, Phys. Chem. Chem. Phys. 14 (2012) 9343–9349.
[44] C.A. Mirkin, R.L. Letsinger, R.C. Mucic, J.J. Storhoff, Nature 382 (1996).
[45] H.K.M. Tanaka, M. McIntire, R. Castillo-Garza, New technique to observe a time evolution of a gold colloidal system in nanochannels of MCM-41 mesoporous silica using UV–Vis spectroscopy, Microporous Mesoporous Mat. 85 (2005) 374–380.
[46] A. Taleb, C. Petit, M.P. Pileni, Synthesis of highly monodisperse silver nanoparticles from AOT reverse micelles: a way to 2D and 3D self-Organization, Chem. Mater. 9 (1997) 950–959.
[47] A. Henglein, Physicochemical properties of small metal particles in solution: 'microelectrode' reactions, chemisorption, composite metal particles, and the atom-to-metal transition, J. Phys. Chem. 97 (1993) 5457–5471.
[48] M.P. Casaletto, A. Longo, A. Martorana, A. Prestianni, A.M. Venezia, XPS study of supported gold catalysts: the role of Au0 and Au+δ species as active sites, Surf. Interface Anal. 38 (2006) 215–218.
[49] A.M. Visco, F. Neri, G. Neri, A. Donato, C. Milone, S. Galvagno, X-ray photoelectron spectroscopy of Au/Fe2O3 catalysts, Phys. Chem. Chem. Phys. 1 (1999) 2869–2873.
[50] I. Iatsunskyi, M. Kempiński, G. Nowaczyk, M. Jancelewicz, M. Pavlenko, K. Załęski, S. Jurga, Structural and XPS studies of PSi/TiO2 nanocomposites prepared by ALD and Ag-assisted chemical etching, Appl. Surf. Sci. 347 (2015) 777–783.
[51] N.B. Rahna, V. Kalarivalappil, M. Nageri, S.C. Pillai, S.J. Hinder, V. Kumar, B.K. Vijayan, Stability studies of PbS sensitised TiO2 nanotube arrays for visible light photocatalytic applications by X-ray photoelectron spectroscopy (XPS), Mater. Sci. Semicond. Process. 42 (Part 3) (2016) 303–310.
[52] H. Liu, W. Yang, Y. Ma, Y. Cao, J. Yao, J. Zhang, T. Hu, Synthesis and characterization of titania prepared by using a photoassisted sol-gel method, Langmuir 19 (2003) 3001–3005.
[53] R. Sanjinés, H. Tang, H. Berger, F. Gozzo, G. Margaritondo, F. Lévy, Electronic structure of anatase TiO2 oxide, J. Appl. Phys. 75 (1994) 2945–2951.
[54] R. Camposeco, S. Castillo, I. Mejía-Centeno, J. Navarrete, J. Marín, Characterization of physicochemical properties of Pd/TiO2 nanostructured catalysts prepared by the photodeposition method, Mater. Charact. 95 (2014) 201–210.
[55] D. Combita, P. Concepción, A. Corma, Gold catalysts for the synthesis of aromatic azocompounds from nitroaromatics in one step, J. Catal. 311 (2014) 339–349.
[56] G. Richner, J.A. van Bokhoven, Y.-M. Neuhold, M. Makosch, K. Hungerbuhler, In situ infrared monitoring of the solid/liquid catalyst interface during the three-phase hydrogenation of nitrobenzene over nanosized Au on TiO2, Phys. Chem. Chem. Phys. 13 (2011) 12463–12471.
[57] F. Cárdenas-Lizana, D. Lamey, S. Gómez-Quero, N. Perret, L. Kiwi-Minsker, M.A. Keane, Selective three-phase hydrogenation of aromatic nitro-compounds over β-molybdenum nitride, Catal. Today 173 (2011) 53–61.
[58] E. Kim, H.S. Jeong, B.M. Kim, Efficient chemoselective reduction of nitro compounds and olefins using Pd-Pt bimetallic nanoparticles on functionalized multi-wall-carbon nanotubes, Catal. Commun. 45 (2014) 25–29.
[59] C.H. Campos, M. Jofré, C.C. Torres, B. Pawelec, J.L.G. Fierro, P. Reyes, Chemoselective hydrogenation of o-, p- and m-chloronitrobenzene at ambient temperature on Au/Fe2O3 catalysts, Appl. Catal. A: Gen. 482 (2014) 127–136.